

# Synthesis and Characterization of [NaO<sub>3</sub>SOCH<sub>2</sub>CH<sub>2</sub>OSO<sub>3</sub>Na] and Its Anchored Form: Surface-Grafted Acid Groups on Zirconium Hydroxide

James G. C. Shen,<sup>†</sup> Thomas H. Kalantar,<sup>‡</sup> Richard G. Herman,<sup>†</sup>  
James E. Roberts,<sup>†</sup> and Kamil Klier<sup>\*,†</sup>

Department of Chemistry and Zettlemoyer Center for Surface Studies, 6 East Packer Avenue, Lehigh University, Bethlehem, Pennsylvania 18015, and M. E. Pruitt Research Center, Dow Chemical Company, Midland, Michigan 48674

Received June 6, 2001. Revised Manuscript Received September 1, 2001

A disodium 1,2-ethanediol bis(hydrogen sulfate) salt, [NaO<sub>3</sub>SOCH<sub>2</sub>CH<sub>2</sub>OSO<sub>3</sub>Na], has been synthesized and anchored onto zirconium hydroxide to produce a high concentration of solid dual acid sites. The reaction of HCON(CH<sub>3</sub>)<sub>2</sub>·SO<sub>3</sub>, (CH<sub>2</sub>OH)<sub>2</sub>, and NaOH produced a stable [NaO<sub>3</sub>SOCH<sub>2</sub>CH<sub>2</sub>OSO<sub>3</sub>Na] precursor in 40% yield. The [NaO<sub>3</sub>SOCH<sub>2</sub>CH<sub>2</sub>OSO<sub>3</sub>Na] salt was exchanged with NH<sub>4</sub><sup>+</sup> using an NH<sub>4</sub>-R resin followed by impregnation of a zirconium hydroxide slurry, yielding [−O<sub>3</sub>SOCH<sub>2</sub>CH<sub>2</sub>OSO<sub>3</sub>]<sup>2−</sup> anchored on Zr(OH)<sub>4</sub>. The characterization of the samples included high-resolution X-ray photoelectron, near-infrared diffuse reflectance, <sup>1</sup>H NMR, and <sup>13</sup>C magic angle spinning NMR spectroscopies. The results provided evidence of a μ<sub>2</sub>-CH<sub>2</sub>CH<sub>2</sub>- ligand bridged between two −OSO<sub>3</sub>- groups in the precursor and the anchored precursor. The ethyl bridge was removed upon calcination at 500 °C to yield surface-grafted acid groups on zirconia. This material had a surface area of 97 m<sup>2</sup> g<sup>−1</sup> and an acid-exchange capacity of 0.70 mequiv of H<sup>+</sup>/g, corresponding to 7.2 μmol acid sites/m<sup>2</sup>, which was about 50% higher than that of sulfated zirconia prepared by standard methods of impregnation by sulfuric acid or ammonium sulfate.

## Introduction

In recent years, there has been increasing interest in the development of solid acid materials.<sup>1–5</sup> Such materials have extensive applications and scientific value, e.g., tungstena-zirconia,<sup>4</sup> sulfated-zirconia,<sup>6</sup> and Nafion-H<sup>7</sup> with strong acid functionalities were employed as catalytic materials for coupling alcohols to unsymmetrical ethers.<sup>1,8,9</sup> The experimental results, kinetic analyses, and theoretical calculations suggest that the

mechanism of the ether syntheses from alcohols is a dual site S<sub>N</sub>2 reaction pathway involving competitive adsorption of reactants on surface Brønsted acid sites.<sup>1,8–12</sup> For this purpose, sulfate deposition on metal oxide was carried out using a traditional impregnation method.<sup>2,4,6</sup> Although this technique has been successful, the concentration of surface acid groups was low (~12% of surface coverage), as determined by N 1s X-ray photoelectron spectroscopy of the conjugate pyridine base titrated to the acid groups.

The catalytic effects in the coupling of alcohols might involve the dispersion of surface acid species, contributions of the surface hydroxyl groups, and acid–base electron-transfer interactions between the support and grafted species.<sup>1,8–11</sup> However, design and successful preparation of solid catalysts with close dual acid functionalities has not been demonstrated until our recent communication.<sup>11</sup> In this regard, our present research focuses on the design and synthesis of [NaO<sub>3</sub>-

\* To whom correspondence should be addressed.

<sup>†</sup> Lehigh University.

<sup>‡</sup> Dow Chemical Co.

(1) (a) Nunan, J.; Klier, K.; Herman, R. G. *J. Chem. Soc., Chem. Commun.* **1985**, 676. (b) Nunan, J. G.; Klier, K.; Herman, R. G. *J. Catal.* **1993**, *139*, 406. (c) Feeley, O. C.; Sun, Q.; Herman, R. G.; Johansson, M.; Lietti, L.; Klier, K. *Catal. Lett.* **1995**, *35*, 13.

(2) (a) Olah, G. A.; Suty Parkash, G. K.; Sommer, J. *Superacids*; John Wiley & Sons: New York, 1985; p 53. (b) Tanabe, K.; Misono, M.; Ono, Y.; Hattori, H. In *New Solid Acids and Bases*; Delmon, B., Yates, J. T., Eds.; Elsevier: Amsterdam, 1989.

(3) (a) Yamaguchi, T.; Jin, T.; Tanabe, K. *J. Phys. Chem.* **1986**, *90*, 3148. (b) Jin, T.; Yamaguchi, T.; Tanabe, K. *J. Phys. Chem.* **1986**, *90*, 4794.

(4) (a) Scheithauer, M.; Grasselli, R. K.; Knözinger, H. *Langmuir* **1998**, *14*, 3019. (b) Boyse, R. A.; Ko, E. I. *J. Catal.* **1998**, *179*, 100. (c) Barton, D. G.; Soled, S. L.; Meitzner, G. D.; Fuentes, G. A.; Iglesia, E. *J. Catal.* **1999**, *181*, 57.

(5) (a) Margolese, D.; Melero, J. A.; Christiansen, S. C.; Chmelka, B. F.; Stucky, G. D. *Chem. Mater.* **2000**, *12*, 2448. (b) Ciesla, U.; Fröba, M.; Stucky, G. D.; Schüth, F. *Chem. Mater.* **1999**, *11*, 227.

(6) (a) Hino, M.; Kobayashi, S.; Arata, K. *J. Am. Chem. Soc.* **1979**, *101*, 6439. (b) Hino, M.; Arata, K. *J. Chem. Soc., Chem. Commun.* **1980**, 851.

(7) (a) Olah, G. A.; Kaspi, J.; Bukala, J. *J. Org. Chem.* **1977**, *42*, 4187. (b) Kaspi, J.; Montgomery, D. D.; Olah, G. A. *J. Org. Chem.* **1978**, *43*, 3147.

(8) Klier, K.; Kwon, H. H.; Herman, R. G.; Hunsicker, R. A.; Ma, Q.; Bollinger, S. J. In *12th International Congress Catalysis*; Corma, A., Melo, F. V., Mendioroz, A., Fierro, F. L. S., Eds.; Elsevier: Amsterdam, 2000; p 3447.

(9) (a) Klier, K.; Herman, R. G.; Johansson, M. A.; Feeley, O. C. *Prepr., Div. Fuel Chem., Am. Chem. Soc.* **1992**, *37(1)*, 236. (b) Feeley, O. C.; Johansson, M. A.; Herman, R. G.; Klier, K. *Prepr., Div. Fuel Chem., Am. Chem. Soc.* **1992**, *37(4)*, 343. (c) Herman, R. G.; Klier, K.; Feeley, O. C.; Johansson, M. A. *Prepr., Div. Fuel Chem., Am. Chem. Soc.* **1994**, *39(2)*, 343.

(10) Sun, Q.; Lietti, L.; Herman, R. G.; Klier, K. *Prepr., Div. Fuel Chem., Am. Chem. Soc.* **1995**, *40(1)*, 138.

(11) Shen, J. G. C.; Kalantar, T. H.; Ma, Q.; Herman, R. G.; Klier, K. *J. Chem. Soc., Chem. Commun.* **2001**, 653.

SOCH<sub>2</sub>CH<sub>2</sub>OSO<sub>3</sub>Na] (a compound possessing double sulfate groups coordinated to an ethanediol (–OCH<sub>2</sub>–CH<sub>2</sub>O–) bridge), anchoring of the [–O<sub>3</sub>SOCH<sub>2</sub>CH<sub>2</sub>O<sub>3</sub>–SO–]<sup>2–</sup> group on zirconium hydroxide, and subsequent decomposition to the surface-grafted acid groups on the supports. The structure, composition, and chemical properties of the precursor and the synthetic solid acid materials were determined using near-infrared diffuse reflectance spectroscopy (NIR-DRS), high-resolution X-ray photoelectron spectroscopy (HR-XPS), <sup>1</sup>H NMR and <sup>13</sup>C solid-state magic angle spinning (MAS) NMR spectroscopies, Merck molecular force field (MMFF)<sup>13</sup> simulation, BET surface area measurement,<sup>14</sup> and solid acid-titration technique.<sup>6,15</sup>

## Experimental Section

**I. Sample Preparation.** *a. Precursor.* A 11.9 g portion of HCON(CH<sub>3</sub>)<sub>2</sub>·SO<sub>3</sub> complex (DMF·SO<sub>3</sub>, Aldrich) and 75 mL of CCl<sub>4</sub> (Aldrich, HPLC grade) were placed in a N<sub>2</sub>-purged, round-bottom flask equipped with a magnetic stir bar. Ethylene glycol (2.0 mL) (Aldrich, anhydrous) was then added dropwise by syringe under stirring over 20 min at room temperature. A clear insoluble oil formed, and the mixture was stirred under N<sub>2</sub> for an additional 2 h. After the oil settled, the CCl<sub>4</sub> was decanted and discarded. Water (50 mL) was added to the oil, followed immediately by ~7 g of aqueous NaOH (50 wt %) until the solution pH reached ~9–10. Ethanol (100–150 mL) was added, and the mixture was evaporated using a rotary evaporator to obtain a white solid. The solid was dissolved in ~100 mL of H<sub>2</sub>O, and enough ethanol was added to begin precipitation. About 1 g of a white solid was collected by filtration and discarded. The filtrate was evaporated to dryness and redissolved in ~30 mL of H<sub>2</sub>O, and the product was precipitated by adding ~50 mL of ethanol. The white microcrystalline solid was isolated by filtration and dried in a vacuum. The resulting product is denoted as the precursor.

*b. The Anchored Precursor.* R–H resin (50 mmol Rexyn 101, 7.7 mequiv g<sup>–1</sup>, Fisher) was cation-exchanged with 75 mL of 70 mmol (NH<sub>4</sub>)<sub>2</sub>SO<sub>4</sub> (Aldrich, 99.99% purity) solution over a cation column, to obtain a NH<sub>4</sub><sup>+</sup> form of the resin. R–NH<sub>4</sub> (5.0 mmol) resin was then cation-exchanged with 1.88 mmol (9.4 mM, 200 mL) of the synthesized precursor, to yield an aqueous solution containing the ammonium form of the precursor. Zirconium hydroxide (13.5 mmol, Aldrich, 97% purity) was immersed into the solution of the ammonium precursor (9.4 mM, 200 mL) with stirring. The mixed solution was equilibrated for 2 h under stirring at room temperature, filtered, washed free of NH<sub>4</sub><sup>+</sup> ions with copious amounts of deionized H<sub>2</sub>O, and dried in ambient air. The resulting white sample is a precursor anchored on the “host” Zr(OH)<sub>4</sub> matrix, which is denoted as the anchored precursor.

*c. The Surface-Grafted Acid Groups.* The anchored precursor was calcined at 500 °C for 3 h to produce surface-grafted acid groups on the zirconia support.

**II. Characterization of Samples.** *a. NIR-DRS.* NIR-DR spectra were recorded using a Varian Cary 5E UV–vis NIR spectrophotometer with a diffuse reflectance attachment with an integration sphere. The powder samples were mounted in a quartz cell with a Suprasil window and measured in the NIR region of 1000–2300 nm at room temperature with 50–120 co-added scans at 2 cm<sup>–1</sup> resolution. A Halon white reflectance standard was used to obtain the baseline. The spectra were evaluated by the Schuster–Kubelka–Munk (SKM) function that gives the ratio of the absorption (*K*) to the scattering (*S*) coefficients as

$$K/S = (1 - R_{\infty})^2 / 2R_{\infty} \quad (1)$$

where *R*<sub>∞</sub> is the ratio of the intensities of light reflected from the sample and the standard.<sup>16</sup>

*b. HR-XPS.* HR-XPS measurements were carried out using the Scienta ESCA-300 photoelectron spectrometer at Lehigh University.<sup>17</sup> This instrument utilizes a water-cooled rotating Al Kα anode to generate an unpolarized 7.6 kW X-ray flux (*hν* = 1486.8 eV), which is monochromatized by seven toroidally bent quartz crystals. Both survey and high-resolution scans of the samples were performed at 5 × 10<sup>–9</sup> Torr in the analysis chamber. The Zr 3d, S 2p, O 1s, C 1s, Na 1s, and N 1s spectral regions were recorded with 150 eV pass energy, an incremental step size of 0.05 eV, and a 0.8 mm slit width. Because the samples were nonconducting, a hot filament gun set at 1.3 eV was employed during the measurements to supply electrons for charge compensation and to improve the resolution.<sup>17</sup>

*c. Quantitative Analysis of HR-XPS Data.* Dreiling,<sup>18a</sup> Vedage et al.,<sup>18b</sup> and Himelfarb<sup>18b</sup> have developed a model based on exponential attenuation of the photoelectron intensity to study the surface overlayers in powders. The peak areas in the XPS spectra were obtained by curve-fitting using the Scienta program.<sup>19</sup> The sensitivity factors were determined by extensive calibration based on modified photoionization cross sections.<sup>20</sup> A quantitative analysis of the surface atomic ratios of S/C and S/Na in the precursor was conducted in terms of the peak areas and the sensitivity factors.<sup>19,21</sup> The surface atomic ratio of S/Zr (*X*<sub>S</sub>/*X*<sub>Zr</sub>) in the anchored precursor was determined using eq 2<sup>18,19,21</sup>

$$(X_S/X_{Zr})_{\text{surface}} = (I_S g \lambda_{Zr} / I_{Zr} t_{Zr}^0) / [(\sigma_S E_{Zr} / \sigma_{Zr} E_S) + (t_S^0 I_S / t_{Zr}^0 I_{Zr})] \quad (2)$$

where *g* is the escape angular factor, 0.75,<sup>22</sup> *I* is the measured photoelectron intensity, *t*<sub>S</sub><sup>0</sup> is the sulfate ion size in the overlayer, 0.488 nm,<sup>23</sup> and *t*<sub>Zr</sub><sup>0</sup> is the monolayer thickness in bulk zirconium hydroxide, 0.182 nm.<sup>21</sup> The S and Zr photoelectron cross sections, *σ*<sub>S</sub> and *σ*<sub>Zr</sub>, are 7.04 and 1.679, respectively<sup>19,21</sup> and the S 2s and Zr 3d kinetic energies, *E*<sub>S</sub> and *E*<sub>Zr</sub>, are 1316.7 and 1303.4 eV, respectively.<sup>19,21</sup> The escape depth, *λ*<sub>Zr</sub>, of photoelectrons of kinetic energy *E*<sub>Zr</sub> was calculated to equal 1.315 nm using Chang's empirical relationship<sup>24</sup>

$$\lambda_{Zr} = 0.2 E_{Zr}^{1/2} t_{Zr}^0 \quad (3)$$

*d. <sup>1</sup>H NMR and <sup>13</sup>C Solid-State MAS NMR Spectroscopies.* Solution-state <sup>1</sup>H NMR spectra of the samples were recorded at 400 MHz using standard library pulse sequences and D<sub>2</sub>O solution. <sup>13</sup>C solid-state MAS NMR spectra were recorded with a GN-300 spectrometer operating at 75.47 MHz. A DOTY Scientific double-tuned 7 mm double air-bearing probe allowed spinning frequencies up to 5 kHz. Samples were loaded in ambient conditions with 25–50 mg of *N*-acetyl glycine as an internal standard. The measurements were carried out at room temperature using 3.5 μs pulse lengths (one-pulse experiments), 3.0 kHz spinning speed, and a 60 s empirically

(16) (a) The discussion of the validity of the SKM theory is given in Kortüm, G. *Reflectance Spectroscopy*; Springer-Verlag: New York, 1969; pp 103–127, 170–216. (b) Klier, K. *J. Opt. Soc. Am.* **1972**, *62*, 882.

(17) Chaney, R. L.; Simmons, G. W. *R&D Mag.* **1990**, *83*.

(18) (a) Dreiling, M. J. *Surf. Sci.* **1978**, *71*, 231. (b) Himelfarb, P. B. Ph.D. Thesis, Lehigh University, Bethlehem, PA, 1986.

(19) Johansson, M.; Klier, K. *Top. Catal.* **1997**, *4*, 99.

(20) Scofield, J. H. *J. Electron Spectrosc. Relat. Phenom.* **1976**, *8*, 129.

(21) Johansson, M. Ph.D. Thesis, Lehigh University, Bethlehem, PA, 1995.

(22) Vedage, G. A.; Himelfarb, P. B.; Simmons, G. W.; Klier, K. *ACS Symp. Ser.* **1985**, *279*, 295.

(23) Huheey, J. E.; Keiter, E. A.; Keiter, R. L. *Inorganic Chemistry: Principles of Structure and Reactivity*, 4th ed.; Harper Collins College Publishers: New York, 1993.

(24) Chang, C. C. *Surf. Sci.* **1975**, *48*, 9.

(12) Streitweiser, A.; Heathcock, C. H. *Introduction to Organic Chemistry*, 2nd ed.; Macmillan: New York, 1981; p 162.

(13) Merck Molecular Force Field Program, 1994.

(14) Brunauer, S.; Emmett, P. H.; Teller, E. *J. Am. Chem. Soc.* **1938**, *60*, 309.

(15) Forni, L. *Catal. Rev.* **1973**, *8*(1), 65.

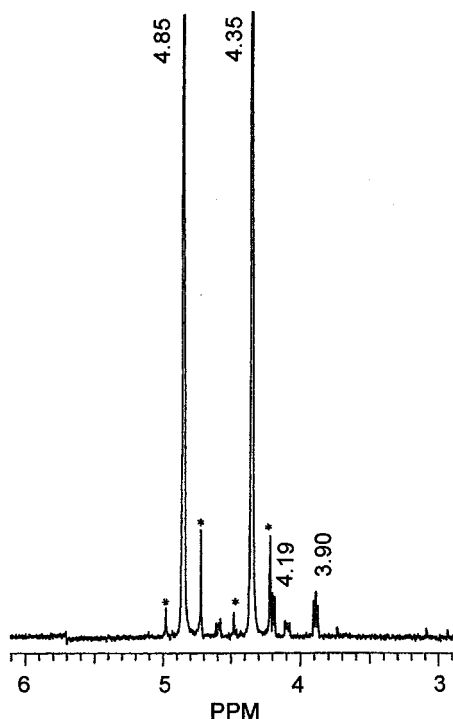


**Figure 1.** 400 MHz <sup>1</sup>H NMR spectrum of the precursor.

determined relaxation delay. Conventional one-pulse and single-contact cross-polarization experiments were employed with proton decoupling during data acquisition.

*e. Determination of Surface Area and Acid-Exchange Capacities.* The surface area of the samples was measured with a Gemini 2360 surface area analyzer using the BET method.<sup>14</sup> The acid-exchange capacities of the sample were determined using a solid acid-titration technique.<sup>6,15,21</sup> In a typical experiment, 0.05 g of solid sample was added to NaCl aqueous solution (2 M, 15 mL). The resulting suspension was allowed to equilibrate and was thereafter titrated potentiometrically by dropwise addition of 0.01 M NaOH aqueous solution.

## Results and Discussion

### I. <sup>1</sup>H NMR and <sup>13</sup>C Solid-State MAS NMR Characterization of the Precursor and the Anchored Precursor.

*a. <sup>1</sup>H NMR Studies of the Precursor.* The <sup>1</sup>H NMR spectrum of the synthetic precursor in D<sub>2</sub>O solution shows two peaks, at 4.85 and 4.35 ppm, and two groups of narrow peaks, centered at 4.19 and 3.90 ppm (Figure 1). The strong <sup>1</sup>H resonance signal at 4.35 ppm is assigned to the [NaO<sub>3</sub>SOCH<sub>2</sub>CH<sub>2</sub>OSO<sub>3</sub>Na] ethyl species,<sup>25</sup> while another <sup>1</sup>H signal at 4.85 ppm is that of HDO. A small amount of <sup>1</sup>H signal intensity of [NaO<sub>3</sub>SOCH<sub>2</sub>CH<sub>2</sub>OSO<sub>3</sub>Na] and HDO species appears in the spinning sidebands, as indicated by asterisks in Figure 1. The lower intensity <sup>1</sup>H signals around 4.19 and 3.90 ppm are attributed to a monosulfate species such as [HOCH<sub>2</sub>CH<sub>2</sub>OSO<sub>3</sub>Na].<sup>25</sup> The <sup>1</sup>H intensities confirm that [NaO<sub>3</sub>SOCH<sub>2</sub>CH<sub>2</sub>OSO<sub>3</sub>Na] was 96% of the organic compounds present in the precursor.

*b. <sup>13</sup>C MAS NMR Studies of the Precursor and the Anchored Precursor.* The <sup>13</sup>C solid-state MAS NMR spectrum of the precursor in Figure 2, curve a, shows a high-intensity narrow peak at 67.54 ppm, which is very close to the <sup>13</sup>C signal of C<sub>α</sub> in tetrahydrofuran (C<sub>4</sub>H<sub>8</sub>O)

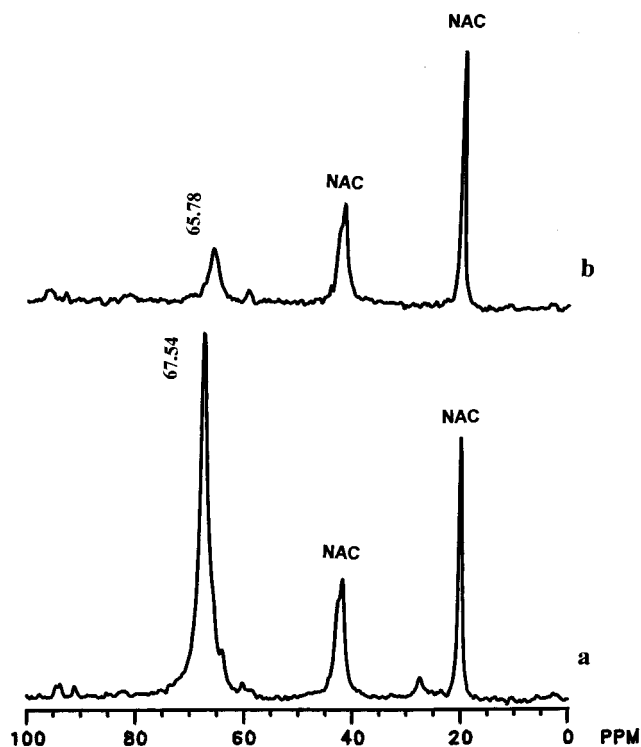


**Figure 2.** <sup>13</sup>C solid-state MAS NMR spectra of (a) the precursor and (b) the precursor anchored on Zr(OH)<sub>4</sub> supports. The peaks labeled NAC arise from the *N*-acetyl glycine internal standard.

at 68 ppm.<sup>25</sup> The single <sup>13</sup>C resonance signal indicates an equivalent chemical environment of the two adjacent carbons in the -CH<sub>2</sub>CH<sub>2</sub>- group. Thus, the <sup>13</sup>C MAS NMR signal at 67.54 ppm is assigned to the μ<sub>2</sub>-CH<sub>2</sub>-CH<sub>2</sub>- group of the precursor.

The anchored precursor yields a <sup>13</sup>C MAS NMR signal at 65.78 ppm (Figure 2, curve b), which is analogous to that of the precursor. This suggests that the μ<sub>2</sub>-CH<sub>2</sub>-CH<sub>2</sub>- group remained intact in the anchored precursor. However, the <sup>13</sup>C resonance peak of the anchored precursor gave a lower intensity and a small upfield shift (67.54 → 65.78 ppm in Figure 2, curves a and b), in comparison with that of the sodium precursor salt, [NaO<sub>3</sub>SO-CH<sub>2</sub>CH<sub>2</sub>-OSO<sub>3</sub>Na]. The lower intensity arising from the anchored precursor is expected due to the dilution effect upon bonding to the support. This is consistent with the inference that the chemical environment around the μ<sub>2</sub>-CH<sub>2</sub>CH<sub>2</sub>- group has changed upon anchoring.

### II. NIR-DRS Characterization of the Precursor and the Anchored Precursor and MMFF Simulation of the C-H Vibrations.

Figure 3, spectrum a, shows four NIR-DR C-H bands of the precursor at 5611, 5692, 5845, and 6012 cm<sup>-1</sup>, and spectrum b exhibits four other C-H peaks of the anchored precursor at 5622, 5717, 5829, and 5995 cm<sup>-1</sup>. With the use of the identifications assigned by <sup>1</sup>H NMR and <sup>13</sup>C MAS NMR, it was proposed that these peaks are ascribed to the C-H overtone and combination bands of the μ<sub>2</sub>-CH<sub>2</sub>-CH<sub>2</sub>- group. To confirm further the assignment of the C-H bands in Figure 3, fundamental vibrational frequencies of [NaO<sub>3</sub>SOCH<sub>2</sub>CH<sub>2</sub>OSO<sub>3</sub>Na] were calculated with the use of the MMFF94 package.<sup>13</sup> The bridging μ<sub>2</sub>-CH<sub>2</sub>CH<sub>2</sub>- ligand is expected to yield four fundamen-

(25) Kemp W. *NMR in Chemistry*; Macmillan Publishing Co.: New York, 1988.

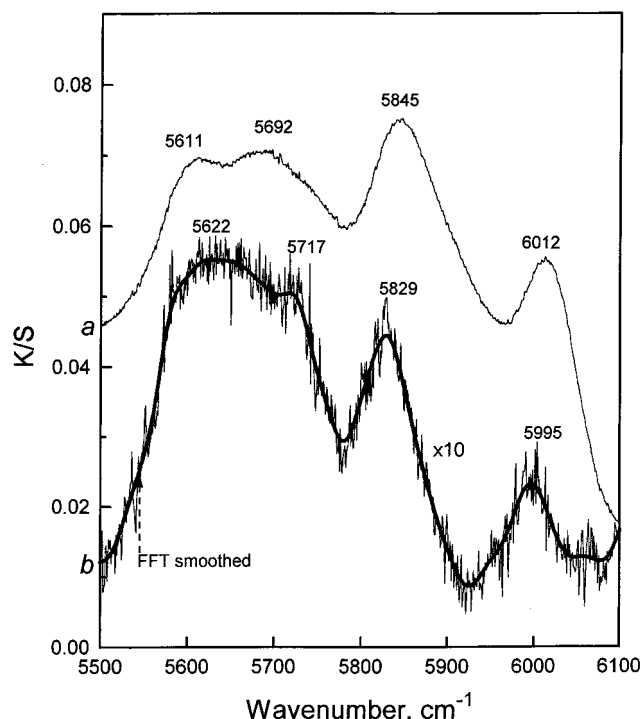


**Figure 3.** Near-infrared diffuse reflectance spectra of (a) the precursor and (b) the precursor anchored on  $\text{Zr}(\text{OH})_4$  supports.

**Table 1. The Calculated and Observed C–H Stretching Frequencies of the  $\mu_2\text{-CH}_2\text{CH}_2\text{-}$  Group in the  $[\text{NaO}_3\text{SO-CH}_2\text{CH}_2\text{-OSO}_3\text{Na}]$  Molecule, the Free Precursor, and the Anchored Precursor**

model or sample	fundamental frequencies, $\text{cm}^{-1}$ <sup>a</sup>	combination bands, $\text{cm}^{-1}$	assignment
$[\text{NaO}_3\text{SO-CH}_2\text{-CH}_2\text{-OSO}_3\text{Na}]$	2913, $\nu_1$ (S + S)	5834 <sup>a</sup>	$(\nu_1 + \nu_2)$
	2921, $\nu_2$ (S – S)	5905 <sup>a</sup>	$(\nu_1 + \nu_3)$
	2992, $\nu_3$ (A + A)	5906 <sup>a</sup>	$(\nu_1 + \nu_4)$
	2993, $\nu_4$ (A – A)	5913 <sup>a</sup>	$(\nu_2 + \nu_3)$
precursor		5914 <sup>a</sup>	$(\nu_2 + \nu_4)$
		5985 <sup>a</sup>	$(\nu_3 + \nu_4)$
		5611 <sup>b</sup>	$(\nu_1 + \nu_2)$
		5692 <sup>b</sup>	$(\nu_1 + \nu_3), (\nu_1 + \nu_4)$
		5845 <sup>b</sup>	$(\nu_2 + \nu_3), (\nu_2 + \nu_4)$
anchored precursor		6012 <sup>b</sup>	$(\nu_3 + \nu_4)$
		5622 <sup>b</sup>	$(\nu_1 + \nu_2)$
		5717 <sup>b</sup>	$(\nu_1 + \nu_3), (\nu_1 + \nu_4)$
		5829 <sup>b</sup>	$(\nu_2 + \nu_3), (\nu_2 + \nu_4)$
ethylene glycol soaked in MgO		5995 <sup>b</sup>	$(\nu_3 + \nu_4)$
		5679 <sup>b</sup>	$(\nu_1 + \nu_2)$
		5848 <sup>b</sup>	$(\nu_1 + \nu_3), (\nu_1 + \nu_4)$
		6333 <sup>b</sup>	$(\nu_2 + \nu_3), (\nu_2 + \nu_4)$
	6798 <sup>b</sup>	$(\nu_3 + \nu_4)$	

<sup>a</sup> The calculated bands. <sup>b</sup> The observed bands.

tal stretching frequencies in the C–H region as listed in Table 1,  $\nu_1$  at 2913  $\text{cm}^{-1}$  (S + S),  $\nu_2$  at 2921  $\text{cm}^{-1}$  (S – S),  $\nu_3$  at 2992  $\text{cm}^{-1}$  (A + A), and  $\nu_4$  at 2993  $\text{cm}^{-1}$  (A – A). The S and A symbols in parentheses denote the symmetric and antisymmetric modes of separate  $\text{CH}_2$  moieties, while the + and – signs represent in-phase and out-of-phase coupling of vibrations of the two  $\text{CH}_2$  moieties in the  $\mu_2\text{-CH}_2\text{CH}_2\text{-}$  link. With the  $\mu_2\text{-CH}_2\text{CH}_2\text{-}$  bridge symmetry being approximated as  $C_{2v}$ , these four vibrations correspond to  $A_1(\nu_1)$ ,  $B_1(\nu_2)$ ,  $B_2(\nu_3)$ , and  $A_2(\nu_4)$  modes.

These four fundamental vibrations can combine into three overtone and combination band regions in the NIR spectrum. The region of interest of the combination

bands and assignments are shown in Table 1, i.e., 5834 ( $\nu_1 + \nu_2$ ), 5905 ( $\nu_1 + \nu_3$ ), 5906 ( $\nu_1 + \nu_4$ ), 5913 ( $\nu_2 + \nu_3$ ), 5914 ( $\nu_2 + \nu_4$ ), and 5985 ( $\nu_3 + \nu_4$ )  $\text{cm}^{-1}$ . On the basis of the simulated combination models of the C–H stretching vibrations in the  $\mu_2\text{-CH}_2\text{CH}_2\text{-}$  group of  $[\text{NaO}_3\text{-SOCH}_2\text{CH}_2\text{OSO}_3\text{Na}]$  (Table 1) the 5611  $\text{cm}^{-1}$  band in spectrum a and the 5622  $\text{cm}^{-1}$  band in spectrum B of Figure 3 are attributed to the  $(\nu_1 + \nu_2)$  mode of the  $\mu_2\text{-CH}_2\text{CH}_2\text{-}$  group, while the 5692  $\text{cm}^{-1}$  band in spectrum a and 5717  $\text{cm}^{-1}$  in spectrum b arise from an overlap of the  $(\nu_1 + \nu_3)$  and  $(\nu_1 + \nu_4)$  modes. The 6012  $\text{cm}^{-1}$  band in spectrum a and 5995  $\text{cm}^{-1}$  band in spectrum b are ascribed to the  $(\nu_3 + \nu_4)$  mode of the  $\mu_2\text{-CH}_2\text{CH}_2\text{-}$  ligand, and the 5845  $\text{cm}^{-1}$  in spectrum A and 5829  $\text{cm}^{-1}$  in spectrum B are assigned to another overlap band of the  $(\nu_2 + \nu_3)$  and  $(\nu_2 + \nu_4)$  modes (Figure 3 and Table 1). The NIR bands in Figure 3 are also similar to those of ethylene glycol soaked in MgO (5679, 5848, 6333, and 6798  $\text{cm}^{-1}$  in Table 1). Nevertheless, there are differences between the frequencies of the precursor and the MMFF94-simulated combination modes, which are mainly ascribed to the anharmonicities and strong coupling between the adjacent  $\text{CH}_2$  groups in the  $\mu_2\text{-CH}_2\text{CH}_2\text{-}$  ligand. The analyses of  $^1\text{H}$  and  $^{13}\text{C}$  NMR, together with NIR-DR spectra and MMFF simulation, suggest the bridging of two  $-\text{OSO}_3-$  groups in the precursor by the  $-\text{CH}_2\text{CH}_2-$  ligand and an  $[-\text{O}_3\text{SOCH}_2\text{-CH}_2\text{OSO}_3-]^{2-}$  group grafted onto the  $\text{Zr}(\text{OH})_4$  surface in the anchored precursor.

In addition, the NIR-DR spectrum of the precursor showed extremely narrow  $\text{H}_2\text{O}$  overtone bands at 5100  $\text{cm}^{-1}$  ( $\nu_2 + \nu_3$ )<sup>26</sup> with 97  $\text{cm}^{-1}$  fwhm (full width at half-maximum) and 7080  $\text{cm}^{-1}$  ( $\nu_1 + \nu_3$ )<sup>26</sup> with 147  $\text{cm}^{-1}$  fwhm, indicating that crystal water was contained in the precursor.<sup>26,27</sup> The intensities of overtone bands of crystal water greatly decreased on passing to the anchored precursor, indicating loss of the water of crystallization.

**III. HR-XPS Characterization of the Precursor and the Anchored Precursor.** *a. HR-XPS Analysis of the Precursor.* HR-XPS analysis of the precursor was carried out to probe the surface composition. The S 2p<sub>3/2</sub> binding energy at 168.8 eV was used as an internal standard for all peak positions.<sup>17,21</sup> Figure 4a shows the S 2p<sub>3/2</sub> binding energy at 168.80 eV and S 2p<sub>1/2</sub> binding energy at 170.00 eV. Figure 4b shows the C 1s binding energies at 284.97, 286.84, and 288.73 eV, where 286.84 eV corresponds to carbon in a  $\equiv\text{C-O-}$  bond.<sup>28</sup> The binding energies of other elements in the precursor are listed in Table 2. The O 1s binding energies observed at 531.77 and 533.17 eV suggest that the precursor contained two types of sulfur–oxygen bonds, namely, S=O and S–O bonds.<sup>3,6,29</sup> The Na 1s binding energy was found at 1071.48 eV. The peak intensities and atomic ratios in the precursor are presented in Table 2. The Na/S/C ratio (where C is only the carbon from the

(26) Herzberg, G. *Infrared and Raman Spectra*; Van Nostrand Reinhold Co.: New York, 1945; p 281.

(27) Klier, K.; Shen, J. H.; Zettlemyer, A. C. *J. Phys. Chem.* **1973**, *77*, 1458.

(28) Moulder, J. F.; Stickle, W. F.; Sobul, P. E.; Bomben, K. D. *Handbook of X-ray Photoelectron Spectroscopy*; Chastain, J., Ed.; Perkin-Elmer Corp.: Eden Prairie, MN, 1992.

(29) (a) Morterra, C.; Cerrato, G.; Emanuel, C.; Bolis, V. *J. Catal.* **1993**, *142*, 349. (b) Morterra, C.; Cerrato, G.; Bolis, V. *Catal. Today* **1993**, *17*, 505.

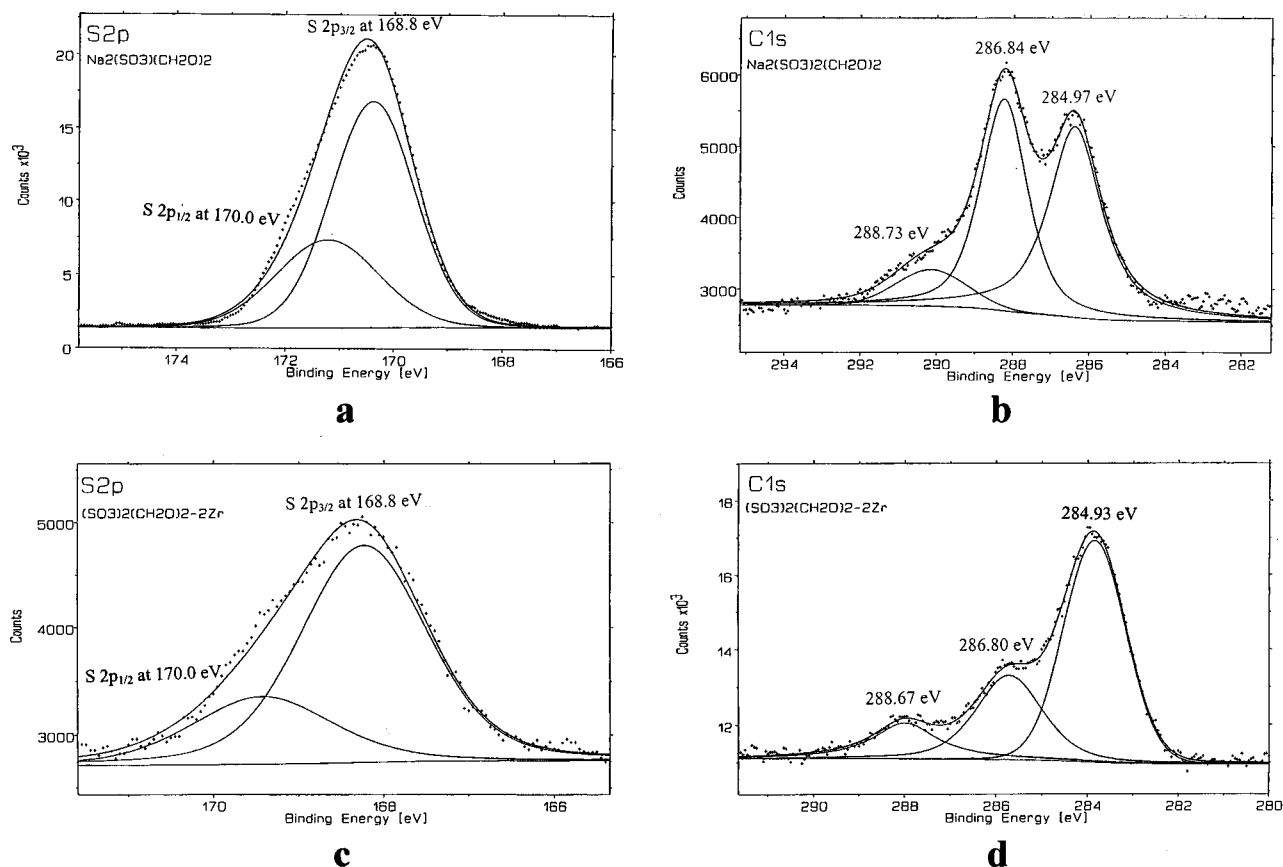


**Figure 4.** HR-XPS spectra of (a) S 2p for the precursor, (b) C 1s for the precursor, (c) S 2p for the anchored precursor, and (d) C 1s for the anchored precursor.

**Table 2.** XPS Binding Energies, Peak Intensities, and Surface Atomic Ratio

precursor				anchored precursor				surface-grafted acid groups			
B. E. (eV)	peak intensity <sup>a</sup>	S/C <sup>b</sup>	S/Na <sup>b</sup>	B. E. (eV)	peak intensity <sup>a</sup>	S/C <sup>b</sup>	S/Zr <sup>c</sup>	B. E. (eV)	peak intensity <sup>a</sup>	S/Zr <sup>c</sup>	O/S <sup>b</sup>
S 2p <sub>total</sub>	2514	1.0:0.3	1.0:1.0		301	1.0:1.0	0.70:1.0		871	0.85	4.40
S 2p <sub>3/2</sub>	168.80			168.80	224			168.80	580		
S 2p <sub>1/2</sub>	170.00			170.00	77			170.00	289		
C 1s <sub>total</sub>	1596				913						
C 1s	284.97			284.93	545						
C 1s	286.84	1.0:0.3		286.80	248	1.0:1.0					
C 1s	288.73			288.67	120						
O 1s <sub>total</sub>	8185				3601				6679		
O 1s				530.14	1496			529.97	2816		
O 1s	531.77			531.61	1474			531.80	3863		4.40
O 1s	533.17			532.72	631						
Na 1s	1071.48		1.0:1.0								
Zr 3d <sub>total</sub>					1623		0.70:1.0		2847	0.85	
Zr 3d <sub>5/2</sub>				182.49	974			182.30	1709		
Zr 3d <sub>3/2</sub>				184.91	656			184.67	1133		

40% [NaOSO<sub>3</sub>-CH<sub>2</sub>CH<sub>2</sub>-OSO<sub>3</sub>Na] + 60% Na<sub>2</sub>SO<sub>4</sub>

[(OH)<sub>3</sub>ZrO<sub>3</sub>SO-CH<sub>2</sub>CH<sub>2</sub>-OSO<sub>3</sub>Zr(OH)<sub>3</sub>]

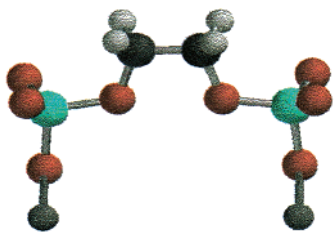
2[(HSO<sub>4</sub>)<sup>-0.85</sup>-ZrO<sub>2</sub>]

<sup>a</sup> Peak intensity = peak area/sensitivity factor. <sup>b</sup> The peak intensity ratio. <sup>c</sup> S/Zr ratio was determined using eq 2.

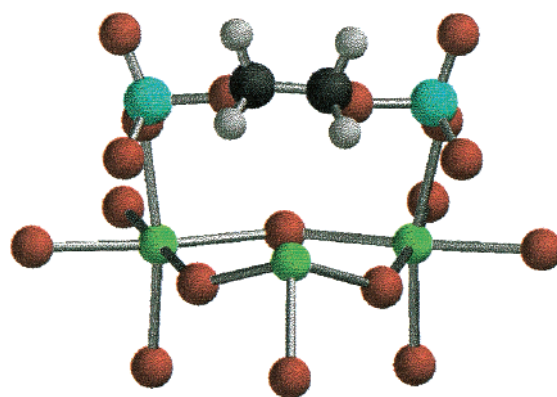
≡C-O- bond) was calculated to be 13.0/10.0/4.0. Assuming that the precursor formula contains  $x$ [NaO<sub>3</sub>-SOCH<sub>2</sub>CH<sub>2</sub>OSO<sub>3</sub>Na] and  $y$ [Na<sub>2</sub>SO<sub>4</sub>], the composition calculated from the Na/S/C ratio indicates that the initial precursor consisted of 40% [NaO<sub>3</sub>-SOCH<sub>2</sub>CH<sub>2</sub>-OSO<sub>3</sub>Na] and 60% [Na<sub>2</sub>SO<sub>4</sub>] (Table 2). This information, together with the <sup>1</sup>H NMR, <sup>13</sup>C MAS NMR, and NIR-DR spectra of the precursor, confirms the structure of the precursor (see Chart 1).

*b. HR-XPS Analysis of the Anchored Precursor.* For the anchored precursor, XPS of S 2p, Zr 3d, O 1s, Na

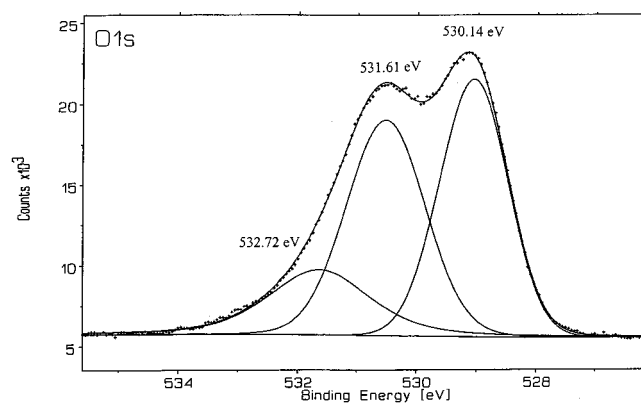
1s, N 1s, and C 1s were investigated. Figure 4c shows the S 2p<sub>3/2</sub> binding energies at 168.8 eV and S 2p<sub>1/2</sub> at 170.0 eV. Figure 4d presents the C 1s binding energy at 286.80 eV, corresponding to carbon of an oxygenated species. The observed binding energies, peak intensities, and concentration of elements in the anchored precursor are listed in Table 2. A 1.0/1.0 atomic ratio of S/C (where C is only the carbon of the ≡C-O- bond species) in the anchored precursor is consistent with the S/C ratio in the [NaO<sub>3</sub>-SO-CH<sub>2</sub>CH<sub>2</sub>-OSO<sub>3</sub>Na] species of the precursor. Three O 1s peaks are observed at 532.72, 531.61,

Chart 1<sup>a</sup>

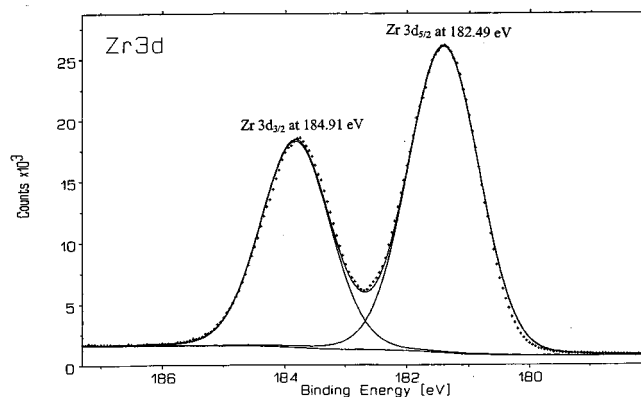
<sup>a</sup> Atom color codes are as follows: C, black; H, light-gray; O, red; S, blue-green; Na, gray.

Chart 2<sup>a</sup>

<sup>a</sup> Atom color codes are as follows: C, black; H, light-gray; O, red; S, blue-green, Zr, green.



a

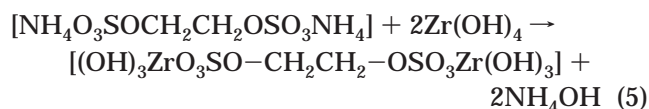
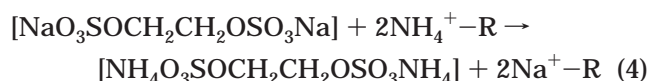


b

**Figure 5.** HR-XPS spectra of (a) O 1s of the anchored precursor and (b) Zr 3d of the anchored precursor.

and 530.14 eV (Figure 5A and Table 2). The lower O 1s binding energy at 530.14 eV is ascribed to the lattice oxygen of the zirconium hydroxide, while the higher O 1s binding energies at 531.61 and 532.72 eV correspond to the oxygens of the sulfate ester groups.<sup>3,6,19,21,29</sup> Furthermore, the O 1s binding-energy shifts in the  $-\text{OSO}_3-$  group between the precursor and the anchored precursor (531.77–531.61 eV and 533.17–532.72 eV) were observed (Table 2). This implies an interaction between the  $-\text{OSO}_3-$  group and the zirconium. The Zr 3d binding energies are observed at 182.49 and 184.91 eV (Figure 5b and Table 2). The surface atomic ratio of sulfate to zirconium in the anchored precursor was determined from eq 2 to be 0.70/1.0, as shown in Table 2. The Na 1s and N 1s peaks were not found in the XPS spectrum, suggesting that the  $\text{Na}^+$  and  $\text{NH}_4^+$  cations of the precursor were completely removed on passing to the anchored precursor. The stoichiometry of zirco-

nium hydroxide anchoring of the precursor is represented by eqs 4 and 5.



On the basis of the above analysis, the structure of the anchored precursor is proposed to be as in Chart 2.

The anchored precursor was calcined at 500 °C to remove the  $\mu_2$ - $\text{CH}_2\text{CH}_2-$  ligand, resulting in the formation of surface-grafted acid groups  $2[(\text{H}_2\text{SO}_4)^{-(2-y)}_x - \text{ZrO}_2]$  on the zirconia support.<sup>11</sup> The so-functionalized zirconia exhibited 0.71 mmol  $\text{g}^{-1}$  surface sulfur concentration (based on the XPS analysis) and 0.70 meq  $\text{g}^{-1}$  acid-exchange capacity, while the unpromoted  $\text{ZrO}_2$  support exhibited no acid-exchange capacity under the same titration condition. The BET surface area was 97  $\text{m}^2 \text{g}^{-1}$  for the calcined sample, and XPS quantitative determination of the sample yielded the ratios 0.85 for S/Zr and  $\sim 4.0$  for O/S, where O was only the oxygen from the hydrogen sulfonic group. The results suggest that the surface-grafted acid groups correspond to the formula  $2[(\text{HSO}_4)^{-0.85} - \text{ZrO}_2]$  on the surface. Such  $2[(\text{HSO}_4)^{-0.85} - \text{ZrO}_2]$  groups grafted on the zirconia surface possessed proximal acid sites favoring high activity and selective catalysis for the alcohols coupling to ethers.<sup>11</sup>

A sulfated zirconia catalyst prepared by the usual method of impregnation of hydrous zirconium hydroxide,<sup>6</sup> followed by calcination at 620 °C, yielded a surface area of 60  $\text{m}^2 \text{g}^{-1}$  and exhibited surface acidity of 0.25, 0.26, and 0.29 mmol  $\text{g}^{-1}$ , based on S/Zr XPS analysis, chemical analysis, and ion-exchange titration, respectively.<sup>21</sup> These data indicate that all sulfur was on the surface of the catalyst and that every sulfate group was monoprotonated. The same impregnated catalyst calcined only to 500 °C possessed a surface area of 72  $\text{m}^2 \text{g}^{-1}$  and exhibited a concentration of surface acid sites of 0.31 mmol  $\text{g}^{-1}$ , as determined by N 1s XPS analysis of pyridine adsorbed at 150 °C.<sup>21</sup> For these two catalysts,

the concentrations correspond to 4.2–4.8  $\mu\text{mol}$  acid sites/ $\text{m}^2$  of surface. The new  $[(\text{CH}_2\text{OSO}_3\text{Zr}(\text{OH})_3)_2]$ -derived catalyst reported here was tested and compared with the impregnated catalyst calcined at 620 °C, and it was shown that the new catalyst exhibited a 78% higher space time yield of methylisobutyl ether (MIBE) formed by methanol/isobutanol coupling.<sup>11</sup> The new catalyst described here was prepared using the ethanediol bridge to form sulfate acid sites in proximity, and it possessed a surface concentration of acid sites of 7.2–7.3  $\mu\text{mol m}^{-2}$ , which is a 50–74% increase in acid site density over that observed for sulfate-impregnated catalysts. Thus, the increased number of surface acid sites achieved here yielded an improved catalyst for MIBE synthesis.

### Conclusions

The results demonstrated the successful synthesis of the disodium 1,2-ethanediol, bis(hydrogen sulfate) com-

pound and the anchored form on zirconium hydroxide. The HR-XPS, NIR-DR, <sup>1</sup>H NMR, and <sup>13</sup>C solid-state MAS NMR spectra, as well as MMFF simulation, confirm the structure and composition of the samples. The surface-grafted acid groups derived from the anchored precursor showed a high concentration of Brønsted acid sites. This work illustrates a new method for preparing anchored Brønsted acid functionalities on supports, which have utility for surface reactions that proceed by dual acid site mechanism.

**Acknowledgment.** Financial support from the U.S. Department of Energy (DE-FG26-98FT40113 and DE-FG02-01ER15181) is appreciated. Special thanks go to Dr. Alfred C. Miller at Lehigh University for professional and technical assistance with the XPS analyses.

CM010550B